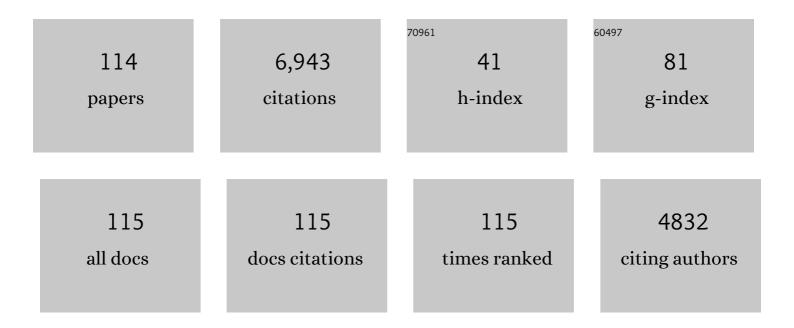
Christiaan van der Tol

List of Publications by Year in descending order

Source: https://exaly.com/author-pdf/3585367/publications.pdf Version: 2024-02-01



#	Article	IF	CITATIONS
1	Linking chlorophyll a fluorescence to photosynthesis for remote sensing applications: mechanisms and challenges. Journal of Experimental Botany, 2014, 65, 4065-4095.	2.4	770
2	An integrated model of soil-canopy spectral radiances, photosynthesis, fluorescence, temperature and energy balance. Biogeosciences, 2009, 6, 3109-3129.	1.3	440
3	Remote sensing of solar-induced chlorophyll fluorescence (SIF) in vegetation: 50†years of progress. Remote Sensing of Environment, 2019, 231, 111177.	4.6	372
4	Models of fluorescence and photosynthesis for interpreting measurements of solarâ€induced chlorophyll fluorescence. Journal of Geophysical Research G: Biogeosciences, 2014, 119, 2312-2327.	1.3	281
5	Quantifying Vegetation Biophysical Variables from Imaging Spectroscopy Data: A Review on Retrieval Methods. Surveys in Geophysics, 2019, 40, 589-629.	2.1	265
6	Far-red sun-induced chlorophyll fluorescence shows ecosystem-specific relationships to gross primary production: An assessment based on observational and modeling approaches. Remote Sensing of Environment, 2015, 166, 91-105.	4.6	263
7	Estimation of vegetation photosynthetic capacity from spaceâ€based measurements of chlorophyll fluorescence for terrestrial biosphere models. Global Change Biology, 2014, 20, 3727-3742.	4.2	260
8	Forest productivity and water stress in Amazonia: observations from GOSAT chlorophyll fluorescence. Proceedings of the Royal Society B: Biological Sciences, 2013, 280, 20130171.	1.2	245
9	Global sensitivity analysis of the SCOPE model: What drives simulated canopy-leaving sun-induced fluorescence?. Remote Sensing of Environment, 2015, 166, 8-21.	4.6	211
10	Model-based analysis of the relationship between sun-induced chlorophyll fluorescence and gross primary production for remote sensing applications. Remote Sensing of Environment, 2016, 187, 145-155.	4.6	185
11	Linking canopy scattering of far-red sun-induced chlorophyll fluorescence with reflectance. Remote Sensing of Environment, 2018, 209, 456-467.	4.6	172
12	Plant functional traits and canopy structure control the relationship between photosynthetic <scp>CO</scp> ₂ uptake and farâ€red sunâ€induced fluorescence in a Mediterranean grassland under different nutrient availability. New Phytologist, 2017, 214, 1078-1091.	3.5	158
13	A model for chlorophyll fluorescence and photosynthesis at leaf scale. Agricultural and Forest Meteorology, 2009, 149, 96-105.	1.9	157
14	Fluspect-B: A model for leaf fluorescence, reflectance and transmittanceÂspectra. Remote Sensing of Environment, 2016, 186, 596-615.	4.6	147
15	Integration of soil moisture in SEBS for improving evapotranspiration estimation under water stress conditions. Remote Sensing of Environment, 2012, 121, 261-274.	4.6	117
16	Estimating crop primary productivity with Sentinel-2 and Landsat 8 using machine learning methods trained with radiative transfer simulations. Remote Sensing of Environment, 2019, 225, 441-457.	4.6	112
17	Evaluating the predictive power of sun-induced chlorophyll fluorescence to estimate net photosynthesis of vegetation canopies: A SCOPE modeling study. Remote Sensing of Environment, 2016, 176, 139-151.	4.6	111
18	Simulations of chlorophyll fluorescence incorporated into the <scp>C</scp> ommunity <scp>L</scp> and <scp>M</scp> odel version 4. Global Change Biology, 2015, 21, 3469-3477.	4.2	95

#	Article	IF	CITATIONS
19	Extending Fluspect to simulate xanthophyll driven leaf reflectance dynamics. Remote Sensing of Environment, 2018, 211, 345-356.	4.6	92
20	On the relationship between sub-daily instantaneous and daily total gross primary production: Implications for interpreting satellite-based SIF retrievals. Remote Sensing of Environment, 2018, 205, 276-289.	4.6	91
21	A model and measurement comparison of diurnal cycles of sun-induced chlorophyll fluorescence of crops. Remote Sensing of Environment, 2016, 186, 663-677.	4.6	80
22	Hyperspectral radiative transfer modeling to explore the combined retrieval of biophysical parameters and canopy fluorescence from FLEX – Sentinel-3 tandem mission multi-sensor data. Remote Sensing of Environment, 2018, 204, 942-963.	4.6	80
23	Fluorescence Correction Vegetation Index (FCVI): A physically based reflectance index to separate physiological and non-physiological information in far-red sun-induced chlorophyll fluorescence. Remote Sensing of Environment, 2020, 240, 111676.	4.6	78
24	Remote sensing of plant-water relations: An overview and future perspectives. Journal of Plant Physiology, 2018, 227, 3-19.	1.6	70
25	Global transpiration data from sap flow measurements: the SAPFLUXNET database. Earth System Science Data, 2021, 13, 2607-2649.	3.7	65
26	Estimation of forest above-ground biomass using multi-parameter remote sensing data over a cold and arid area. International Journal of Applied Earth Observation and Geoinformation, 2012, 14, 160-168.	1.4	62
27	The mSCOPE model: A simple adaptation to the SCOPE model to describe reflectance, fluorescence and photosynthesis of vertically heterogeneousÂcanopies. Remote Sensing of Environment, 2017, 201, 1-11.	4.6	62
28	Analysis of Red and Far-Red Sun-Induced Chlorophyll Fluorescence and Their Ratio in Different Canopies Based on Observed and Modeled Data. Remote Sensing, 2016, 8, 412.	1.8	59
29	Groundwater and unsaturated zone evaporation and transpiration in a semi-arid open woodland. Journal of Hydrology, 2017, 547, 54-66.	2.3	56
30	Remote Sensing of Grass Response to Drought Stress Using Spectroscopic Techniques and Canopy Reflectance Model Inversion. Remote Sensing, 2016, 8, 557.	1.8	54
31	Using reflectance to explain vegetation biochemical and structural effects on sun-induced chlorophyll fluorescence. Remote Sensing of Environment, 2019, 231, 110996.	4.6	52
32	Heatwave breaks down the linearity between sunâ€induced fluorescence and gross primary production. New Phytologist, 2022, 233, 2415-2428.	3.5	51
33	Impact of land use and land cover transitions and climate on evapotranspiration in the Lake Naivasha Basin, Kenya. Science of the Total Environment, 2019, 682, 19-30.	3.9	50
34	The scattering and re-absorption of red and near-infrared chlorophyll fluorescence in the models Fluspect and SCOPE. Remote Sensing of Environment, 2019, 232, 111292.	4.6	49
35	EAGLE 2006 – Multi-purpose, multi-angle and multi-sensor in-situ and airborne campaigns over grassland and forest. Hydrology and Earth System Sciences, 2009, 13, 833-845.	1.9	48
36	Spatioâ€Temporal Convergence of Maximum Daily Lightâ€Use Efficiency Based on Radiation Absorption by Canopy Chlorophyll. Geophysical Research Letters, 2018, 45, 3508-3519.	1.5	48

#	Article	IF	CITATIONS
37	Integrating satellite optical and thermal infrared observations for improving daily ecosystem functioning estimations during a drought episode. Remote Sensing of Environment, 2018, 209, 375-394.	4.6	45
38	Reference crop evapotranspiration derived from geo-stationary satellite imagery: a case study for the Fogera flood plain, NW-Ethiopia and the Jordan Valley, Jordan. Hydrology and Earth System Sciences, 2010, 14, 2219-2228.	1.9	44
39	FluorWPS: A Monte Carlo ray-tracing model to compute sun-induced chlorophyll fluorescence of three-dimensional canopy. Remote Sensing of Environment, 2016, 187, 385-399.	4.6	43
40	Quantifying the uncertainty in estimates of surface–atmosphere fluxes through joint evaluation of the SEBS and SCOPE models. Hydrology and Earth System Sciences, 2013, 17, 1561-1573.	1.9	42
41	An evaluation of SCOPE: A tool to simulate the directional anisotropy of satellite-measured surface temperatures. Remote Sensing of Environment, 2015, 158, 362-375.	4.6	42
42	Exploring the physiological information of Sun-induced chlorophyll fluorescence through radiative transfer model inversion. Remote Sensing of Environment, 2018, 215, 97-108.	4.6	41
43	Impact of climate change-induced alterations in peatland vegetation phenology and composition on carbon balance. Science of the Total Environment, 2022, 827, 154294.	3.9	41
44	Estimating zero-plane displacement height and aerodynamic roughness length using synthesis of LiDAR and SPOT-5 data. Remote Sensing of Environment, 2011, 115, 2330-2341.	4.6	40
45	Estimating montane forest above-ground biomass in the upper reaches of the Heihe River Basin using Landsat-TM data. International Journal of Remote Sensing, 2014, 35, 7339-7362.	1.3	40
46	Modelling sun-induced fluorescence and photosynthesis with a land surface model at local and regional scales in northern Europe. Biogeosciences, 2017, 14, 1969-1987.	1.3	40
47	SCOPE 2.0: a model to simulate vegetated land surface fluxes and satellite signals. Geoscientific Model Development, 2021, 14, 4697-4712.	1.3	39
48	Average wet canopy evaporation for a Sitka spruce forest derived using the eddy correlation-energy balance technique. Journal of Hydrology, 2003, 276, 12-19.	2.3	38
49	Quantitative Estimation of Fluorescence Parameters for Crop Leaves with Bayesian Inversion. Remote Sensing, 2015, 7, 14179-14199.	1.8	35
50	Multiple-constraint inversion of SCOPE. Evaluating the potential of GPP and SIF for the retrieval of plant functional traits. Remote Sensing of Environment, 2019, 234, 111362.	4.6	35
51	Coupling socio-economic factors and eco-hydrological processes using a cascade-modeling approach. Journal of Hydrology, 2014, 518, 49-59.	2.3	33
52	Modeling forest above-ground biomass dynamics using multi-source data and incorporated models: A case study over the qilian mountains. Agricultural and Forest Meteorology, 2017, 246, 1-14.	1.9	32
53	Unraveling the physical and physiological basis for the solar- induced chlorophyll fluorescence and photosynthesis relationship using continuous leaf and canopy measurements of a corn crop. Biogeosciences, 2021, 18, 441-465.	1.3	32
54	Retrieval of canopy component temperatures through Bayesian inversion of directional thermal measurements. Hydrology and Earth System Sciences, 2009, 13, 1249-1260.	1.9	31

#	Article	IF	CITATIONS
55	Variance-based sensitivity analysis of BIOME-BGC for gross and net primary production. Ecological Modelling, 2014, 292, 26-36.	1.2	28
56	The SPART model: A soil-plant-atmosphere radiative transfer model for satellite measurements in the solar spectrum. Remote Sensing of Environment, 2020, 247, 111870.	4.6	28
57	Validation of remote sensing of bare soil ground heat flux. Remote Sensing of Environment, 2012, 121, 275-286.	4.6	26
58	Representing the root water uptake process in the Common Land Model for better simulating the energy and water vapour fluxes in a Central Asian desert ecosystem. Journal of Hydrology, 2013, 502, 145-155.	2.3	26
59	Estimating photosynthetic capacity from leaf reflectance and Chl fluorescence by coupling radiative transfer to a model for photosynthesis. New Phytologist, 2019, 223, 487-500.	3.5	26
60	Systematic Orbital Geometry-Dependent Variations in Satellite Solar-Induced Fluorescence (SIF) Retrievals. Remote Sensing, 2020, 12, 2346.	1.8	25
61	Characterisation of hydroclimatological trends and variability in the Lake Naivasha basin, Kenya. Hydrological Processes, 2015, 29, 3276-3293.	1.1	24
62	Downscaling of far-red solar-induced chlorophyll fluorescence of different crops from canopy to leaf level using a diurnal data set acquired by the airborne imaging spectrometer HyPlant. Remote Sensing of Environment, 2021, 264, 112609.	4.6	24
63	Testing three approaches to estimate soil evaporation through a dry soil layer in a semi-arid area. Journal of Hydrology, 2018, 567, 405-419.	2.3	23
64	Optimal inverse estimation of ecosystem parameters from observations of carbon and energy fluxes. Biogeosciences, 2019, 16, 77-103.	1.3	23
65	Extending the SCOPE model to combine optical reflectance and soil moisture observations for remote sensing of ecosystem functioning under water stress conditions. Remote Sensing of Environment, 2019, 221, 286-301.	4.6	23
66	Discrete anisotropic radiative transfer modelling of solar-induced chlorophyll fluorescence: Structural impacts in geometrically explicit vegetation canopies. Remote Sensing of Environment, 2021, 263, 112564.	4.6	22
67	Growing season net ecosystem <scp>CO</scp> ₂ exchange of two desert ecosystems with alkaline soils in Kazakhstan. Ecology and Evolution, 2014, 4, 14-26.	0.8	21
68	Global Sensitivity Analysis of the SCOPE Model in Sentinel-3 Bands: Thermal Domain Focus. Remote Sensing, 2019, 11, 2424.	1.8	21
69	Effect of sub-layer corrections on the roughness parameterization of a Douglas fir forest. Agricultural and Forest Meteorology, 2012, 162-163, 115-126.	1.9	19
70	The Complicate Observations and Multi-Parameter Land Information Constructions on Allied Telemetry Experiment (COMPLICATE). PLoS ONE, 2015, 10, e0137545.	1.1	19
71	Nitrogen and Phosphorus effect on Sun-Induced Fluorescence and Gross Primary Productivity in Mediterranean Grassland. Remote Sensing, 2019, 11, 2562.	1.8	19
72	Energy partitioning and its controls over a heterogeneous semiâ€arid shrubland ecosystem in the Lake Naivasha Basin, Kenya. Ecohydrology, 2016, 9, 1358-1375.	1.1	18

#	Article	IF	CITATIONS
73	The influence of long-term changes in canopy structure on rainfall interception loss: a case study in Speulderbos, the Netherlands. Hydrology and Earth System Sciences, 2018, 22, 3701-3719.	1.9	18
74	Hyplant-Derived Sun-Induced Fluorescence—A New Opportunity to Disentangle Complex Vegetation Signals from Diverse Vegetation Types. Remote Sensing, 2019, 11, 1691.	1.8	18
75	Uncertainty analysis of gross primary production partitioned from net ecosystem exchange measurements. Biogeosciences, 2016, 13, 1409-1422.	1.3	16
76	A Bayesian approach to estimate sensible and latent heat over vegetated land surface. Hydrology and Earth System Sciences, 2009, 13, 749-758.	1.9	15
77	senSCOPE: Modeling mixed canopies combining green and brown senesced leaves. Evaluation in a Mediterranean Grassland. Remote Sensing of Environment, 2021, 257, 112352.	4.6	15
78	Topography induced spatial variations in diurnal cycles of assimilation and latent heat of Mediterranean forest. Biogeosciences, 2007, 4, 137-154.	1.3	14
79	Optimum vegetation characteristics, assimilation, and transpiration during a dry season: 1. Model description. Water Resources Research, 2008, 44, .	1.7	14
80	Reprint of: Estimation of forest above-ground biomass using multi-parameter remote sensing data over a cold and arid area. International Journal of Applied Earth Observation and Geoinformation, 2012, 17, 102-110.	1.4	14
81	Retrieval of land surface properties from an annual time series of Landsat TOA radiances during a drought episode using coupled radiative transfer models. Remote Sensing of Environment, 2020, 238, 110917.	4.6	14
82	Integrated modeling of canopy photosynthesis, fluorescence, and the transfer of energy, mass, and momentum in the soil–plant–atmosphere continuum (STEMMUS–SCOPE v1.0.0). Geoscientific Model Development, 2021, 14, 1379-1407.	1.3	14
83	Contact and directional radiative temperature measurements of sunlit and shaded land surface components during the SEN2FLEX 2005 campaign. International Journal of Remote Sensing, 2008, 29, 5183-5192.	1.3	13
84	Decoupling of a Douglas fir canopy: a look into the subcanopy with continuous vertical temperature profiles. Biogeosciences, 2020, 17, 6423-6439.	1.3	13
85	Simulation of Forest Evapotranspiration Using Time-Series Parameterization of the Surface Energy Balance System (SEBS) over the Qilian Mountains. Remote Sensing, 2015, 7, 15822-15843.	1.8	12
86	Meteorological controls on evapotranspiration over a coastal salt marsh ecosystem under tidal influence. Agricultural and Forest Meteorology, 2019, 279, 107755.	1.9	12
87	Improved retrieval of land surface biophysical variables from time series of Sentinel-3 OLCI TOA spectral observations by considering the temporal autocorrelation of surface and atmospheric properties. Remote Sensing of Environment, 2021, 256, 112328.	4.6	12
88	Bayesian integration of flux tower data into a process-based simulator for quantifying uncertainty in simulated output. Geoscientific Model Development, 2018, 11, 83-101.	1.3	11
89	Characterization of a Highly Biodiverse Floodplain Meadow Using Hyperspectral Remote Sensing within a Plant Functional Trait Framework. Remote Sensing, 2016, 8, 112.	1.8	10
90	Unified Four-Stream Radiative Transfer Theory in the Optical-Thermal Domain with Consideration of Fluorescence for Multi-Layer Vegetation Canopies. Remote Sensing, 2020, 12, 3914.	1.8	10

#	Article	IF	CITATIONS
91	On the seasonal relation of sun-induced chlorophyll fluorescence and transpiration in a temperate mixed forest. Agricultural and Forest Meteorology, 2021, 304-305, 108386.	1.9	10
92	An Overview of the Regional Experiments for Land-atmosphere Exchanges 2012 (REFLEX 2012) Campaign. Acta Geophysica, 2015, 63, 1465-1484.	1.0	9
93	Spatial Patterns and Temporal Stability of Throughfall in a Mature Douglas-fir Forest. Water (Switzerland), 2018, 10, 317.	1.2	9
94	Modelling hourly evapotranspiration in urban environments with SCOPE using open remote sensing and meteorological data. Hydrology and Earth System Sciences, 2022, 26, 1111-1129.	1.9	8
95	Automated Directional Measurement System for the Acquisition of Thermal Radiative Measurements of Vegetative Canopies. Sensors, 2009, 9, 1409-1422.	2.1	7
96	A simple method using climatic variables to estimate canopy temperature, sensible and latent heat fluxes in a winter wheat field on the North China Plain. Hydrological Processes, 2009, 23, 665-674.	1.1	7
97	An Analysis of Turbulent Heat Fluxes and the Energy Balance During the REFLEX Campaign. Acta Geophysica, 2015, 63, 1516-1539.	1.0	5
98	Google Earth Engine Sentinel-3 OLCI Level-1 Dataset Deviates from the Original Data: Causes and Consequences. Remote Sensing, 2021, 13, 1098.	1.8	5
99	Year-long, broad-band, microwave backscatter observations of an alpine meadow over the Tibetan Plateau with a ground-based scatterometer. Earth System Science Data, 2021, 13, 2819-2856.	3.7	5
100	Can we retrieve vegetation photosynthetic capacity paramter from solar-induced fluorescence?. , 2016, , .		3
101	Dynamic analysis and modeling of Forest above-ground biomass. , 2014, , .		2
102	Modeling Reflectance, Fluorescence and Photosynthesis: Development of the Scope Model. , 2018, , .		2
103	Modeling hydrological response to land use/cover change: case study of Chirah Watershed (Soan) Tj ETQq1 1 C).784314 rg 0.6	gBT_/Overloci
104	Quantitative global mapping of terrestrial vegetation photosynthesis: The Fluorescence Explorer (FLEX) mission. , 2017, , .		1
105	Broadband Full Polarimetric Scatterometry for Monitoring Soil Moisture and Vegetation Properties Over a Tibetan Meadow. , 2018, , .		1
106	Mapping of biophysical and biochemical properties of coastal tidal wetland habitats with Landsat 8. Journal of Applied Remote Sensing, 2021, 15, .	0.6	1
107	Scaling photosynthetic function and CO2 dynamics from leaf to canopy level for maize – dataset combining diurnal and seasonal measurements of vegetation fluorescence, reflectance and vegetation indices with canopy gross ecosystem productivity. Data in Brief, 2021, 39, 107600.	0.5	1
108	Regional forest above-ground biomass retrieval by optimized k-NN algorithm in Northeast China. , 2013,		0

,.

#	ARTICLE	IF	CITATIONS
109	Global sensitivity analysis of the A-SCOPE model in support of future FLEX fluorescence retrievals. , 2014, , .		0
110	Sensitivity of scope modelled GPP and fluorescence for different plant functional types. , 2014, , .		0
111	Photosynthesis-Sun Induced Fluorescence Relationship in a Mediterranean Grassland. , 2018, , .		0
112	A Spectral Invariant Approach to Modelling Radiative Transfer Of Sun-Induced Chlorophyll Fluorescence. , 2018, , .		0
113	Estimation of Vegetation Functioning in a Drought Episode from Optical and Thermal Remote Sensing. , 2018, , .		0
114	Multi-model Approach for Spatial Evapotranspiration Mapping: Comparison of Models Performance for Different Ecosystems. , 2014, , 285-305.		0